Measuring Hidden Higgs and Strongly-Interacting Higgs Scenarios

Sebastian Bock,[1] Remi Lafaye,[2] Tilman Plehn,[1] Michael Rauch,[3] Dirk Zerwas,[4] and Peter M. Zerwas[5,6]

[1]*Institut für Theoretische Physik, Universität Heidelberg, Germany*
[2]*LAPP, Universié de Savoie, IN2P3/CNRS, Annecy*
[3]*Institut für Theoretische Physik, Karlsruhe Institute of Technology, Karlsruhe, Germany*
[4]*LAL, IN2P3/CNRS, Orsay, France*
[5]*Deutsches Elektronen-Synchrotron DESY, Hamburg, Germany*
[6]*Institut für Theoretische Teilchenphysik und Kosmologie, RWTH Aachen University, Germany*

(Dated: September 20, 2010)

Higgs couplings can be affected by physics beyond the Standard Model. We study modifications through interactions with a hidden sector and in specific composite Higgs models accessible at the LHC. Both scenarios give rise to congruent patterns of universal, or partially universal, shifts. In addition, Higgs decays to the hidden sector may lead to invisible decay modes which we also exploit. Experimental bounds on such potential modifications will measure the concordance of an observed Higgs boson with the Standard Model.

I. INTRODUCTION

Embedding the Standard Model [SM] into an extended theory will, in general, modify the couplings predicted in the minimal Higgs sector of the Standard Model [1, 2]. Thus, measuring the Higgs couplings at the LHC [3, 4] will shed light on potential scenarios beyond the Standard Model. In two well motivated models the analysis is particularly transparent:

First, theories beyond the Standard Model may include a hidden sector. The Higgs field offers an attractive candidate for opening the portal to such a hidden sector [5–8]. The coupling between the SM-singlet Higgs mass term and the corresponding SM-neutral Higgs term in the hidden sector leads to an interaction which transfers the renormalizability from the Standard Model to the extended theory.

Second, interpreting the Higgs particle as composite pseudo-Goldstone boson generated by new strong interactions is clearly a well motivated scenario [9–12]. The strong interactions will induce deviations from the properties predicted for a minimal point-like Higgs particle so that the Higgs profile may signal dynamical structures beyond the Standard Model.

If the Standard Model Higgs field couples to a hidden Higgs sector, the couplings to the other Standard Model particles are modified universally; in addition, decays into the hidden sector may generate an invisible decay mode and thereby affect the total width. In strong interaction models where the Higgs boson emerges as a pseudo-Goldstone boson all the Higgs couplings, cross sections and partial widths, may be altered universally or following a simple fermion *vs* boson pattern. Moreover, this scenario does not predict any novel invisible decays. The set of these characteristics will allow us to discriminate between the two scenarios.

In general, depending on the operator basis chosen [13–17], some $\mathcal{O}(10)$ free parameters may affect the measured production and decay rates at the LHC. A universal [or partially universal] modification of the Higgs couplings tremendously simplifies the complexity of any experimental analysis to the measurement of just one, or two, new parameters. Furthermore, setting bounds on universal deviations from the Standard Model Higgs couplings measures the degree of concordance between the observed Higgs boson and the Standard Model in a particularly transparent form.

In the two scenarios introduced above, the twin width-ratios of the Higgs boson are modified by a parameter κ:

$$\frac{\Gamma_p \Gamma_d}{\Gamma_{\text{tot}}} = \kappa \left(\frac{\Gamma_p \Gamma_d}{\Gamma_{\text{tot}}} \right)^{\text{SM}} . \tag{1}$$

The partial widths refer to the production channel p and the decay mode d, either exclusively or summing over sets of initial or final states. These ratios are measured, at the Born level, directly by the product of production cross section times decay branching ratio of the process $p \to Higgs \to d$ in the narrow width approximation. In the hidden sector the parameter κ is universal; in the strong interaction scenario we consider it may take different values for Higgs couplings to vector bosons or fermions [12].

For a hidden sector the decay label d includes invisible Higgs decays, *i.e.* the partial width Γ_{hid}. This second parameter can be measured via the invisible branching ratio BR_{inv}. It is well-known [18–21] that the determination of BR_{inv} at hadron colliders is quite demanding, even through it naturally appears in many extensions of the Standard Model, like four lepton generations or supersymmetry [8].

In the present study we will show, adopting the tools of SFitter, at which level κ as well as Γ_{hid}, if present, can be determined at the LHC.

The measurements of κ and BR_{inv} do not require the estimate of the total width appearing in the denominator of Eq.(1). Nevertheless, estimating Γ_{tot} will provide us with consistency checks on our theoretical ansatz. One way is to simply identify the total Higgs width with the sum of all partial widths, with or without invisible channels [4]. The non-observed partial widths are fixed to the Standard Model value scaled by the same global factor applied to the observed partial widths. This method relies strongly on the recent resurrection of the $H \to b\bar{b}$ channel based on fat jet searches [22, 23]. An alternative way to construct an upper limit to the Higgs width — to be combined with the lower limit from all observed partial widths — would be motivated by the unitarization of $WW \to WW$ scattering. The Standard Model Higgs state saturates this unitarization, so modulo quantum corrections the relation $g_{WWH} \lesssim g^{\text{SM}}_{WWH}$ becomes an upper bound to the Higgs width [3]. We cannot use such an additional constraint because the observed scalar state in our models overlaps only partly with the state related to electroweak symmetry breaking.

Extracting Higgs parameters from LHC data [3, 4] forces us to pay attention to the different uncertainties affecting the rate measurements and their comparison to theory predictions for Higgs production [24, 25] and decay [26, 27]. For typical luminosities around 30 fb^{-1} statistical uncertainties will be the limiting factor for example in weak-boson-fusion or Higgs-strahlung channels. Simulating these statistical uncertainties we use Poisson statistics. Experimental systematic errors, as long as they are related to measured properties of the detector, are expected to be dominantly Gaussian. We include flat theory errors based on the Rfit profile-likelihood construction [28, 29].

In part of our studies ratios of Higgs couplings will play a crucial role. Higher precision in measuring these ratios may naively be expected compared with individual measurements of couplings [3]. For such an improvement the analysis should not be statistics dominated, which it largely is however for an integrated luminosity of 30 fb^{-1}. Moreover, while experimental systematic uncertainties tend to cancel between the same Higgs decays but different production channels, the dominant theory errors are expected to cancel for identical production mechanisms. In line with these arguments we have found that using ratios does not significantly improve the results of Higgs sector analyses [4].

In this study we will show how κ as well as Γ_{hid} can be determined using SFitter. Starting from the completely exclusive likelihood map, SFitter determines the best-fitting point in the Higgs-sector parameter space. While a Bayesian probability analysis of the entire Higgs parameter space at the LHC is spoiled by noise, profile likelihoods can be studied in the vicinity of the best-fitting points [4]. In this analysis we assume that we already know the global structure of the likelihood map, so we can focus on the local properties around the SM-like solution. As it will turn out, alternative solutions can be studied nevertheless, for example with sign switches for some of the Higgs couplings.

Technically, the analysis presented in this paper is based on the SFitter-Higgs setup. The Higgs production rates include NLO QCD corrections except for the top-quark associated production mode. For the decays we use a modified version of HDECAY [27], which contains both NLO QCD terms and off-shell decays into vector bosons. For a list of all measurements and their different errors we refer to Ref. [4]. Compared to this previous analysis we have updated the numbers for the $H \to b\bar{b}$ channel in associated production with vector bosons from the recent ATLAS study [23], which confirms the previously obtained significances. The event rates for weak-boson-fusion production with decay into invisible states are adopted from Ref. [19]. The central data set is smeared around the theory predictions according to the theoretical error and the experimental errors, taking into account the correlations among the observables. For each of the toy-experiments we determine the best-fit values. This numerical determination of the resulting parameter uncertainties is fitted to Gaussian distributions.

The new technical aspect of the present study is the more refined approach to the hypotheses tested: if we do not measure all Higgs couplings independently but instead test a given model hypothesis, the limits on the extracted model parameters improve significantly. Because this approach requires fewer measurements we now consider Higgs masses between 110 and 200 GeV and find a significant enhancement of the determination power for 30 fb^{-1} of LHC data at a collider energy of 14 TeV.

II. HIGGS PORTAL TO HIDDEN SECTOR

The Standard Model, or extensions of it, may be connected to a hidden sector. An interesting realization of such a mechanism is provided by specifying the scalar Higgs domains in both sectors as the link between the two sectors [5, 6]. To explore the possibility of detecting a hidden sector at the LHC we investigate a scenario in which the Standard Model Higgs sector is coupled to the hidden Higgs sector through quartic interactions. Such a scalar system is technically transparent and may therefore serve as paradigm for generic experimental features that could signal a hidden sector. There are many variants to this specific scenario, *e.g.* a hidden scalar sector without spontaneous symmetry breaking, large ensembles of scalar fields, etc. The scenarios can be disentangled by analyzing a few characteristic observables of the Higgs particles, in particular Higgs couplings. In this letter we will concentrate on the simplest setup to quantify the potential of experimental analyses at the LHC.

The scenario we will focus on for now is described by the Higgs potential of the Standard Model $[s]$, the isomorphic potential in the hidden sector $[h]$, and the quartic interaction potential coupling the two sectors with strength η_χ, *videlicet*,

$$\mathcal{V} = \mu_s^2|\phi_s|^2 + \lambda_s|\phi_s|^4 \; + \; \mu_h^2|\phi_h|^2 + \lambda_h|\phi_h|^4 \; + \; \eta_\chi|\phi_s|^2|\phi_h|^2 \, . \tag{2}$$

Expanding the two Higgs fields about their vacuum expectation values $\phi_j \to (v_j + H_j)/\sqrt{2}$ we encounter shifts away from the standard values by the interaction term,

$$v_s^2 = \frac{1}{\lambda_s}\left(-\mu_s^2 - \frac{1}{2}\eta_\chi v_h^2\right) \qquad \text{and} \qquad v_h^2 = \frac{1}{\lambda_h}\left(-\mu_h^2 - \frac{1}{2}\eta_\chi v_s^2\right) . \tag{3}$$

The Higgs states in the SM and the hidden sector will be mixed. Diagonalizing the Higgs mass matrix,

$$\mathcal{M}^2 = \begin{pmatrix} 2\lambda_s v_s^2 & \eta_\chi v_s v_h \\ \eta_\chi v_s v_h & 2\lambda_h v_h^2 \end{pmatrix} , \tag{4}$$

generates two mass eigenvalues $M_{1,2}$ and the mixing angle χ

$$\begin{aligned} M_{1,2}^2 &= (\lambda_s v_s^2 + \lambda_h v_h^2) \pm \left[(\lambda_s v_s^2 - \lambda_h v_h^2)^2 + (\eta_\chi v_s v_h)^2\right]^{1/2} \\ \tan 2\chi &= \eta_\chi v_s v_h / [\lambda_s v_s^2 - \lambda_h v_h^2] \end{aligned} \tag{5}$$

for the mass eigenstates

$$\begin{aligned} H_1 = &\quad \cos\chi\, H_s + \sin\chi\, H_h \\ H_2 = &-\sin\chi\, H_s + \cos\chi\, H_h \ . \end{aligned} \tag{6}$$

Both, H_1 and H_2 couple to Standard Model fields through their H_s components and to the hidden sector through the H_h admixtures. To focus on generic features we assume the potential parameters λ_j and v_j to be of similar size and the mixing parameter η_χ to be moderate. The properties of H_1 then remain dominated by the Standard Model component, while the properties of H_2 are characterized primarily by the hidden Higgs component.

The phenomenology of a Higgs portal to the hidden sector depends on whether the standard Higgs particle is lighter or heavier than the new companion. In this study we assume that H_1 is light and mainly decays into Standard Model particles, at a rate reduced by mixing, and with an admixture of invisible decays to the hidden sector. In general, the heavier H_2 bosons decay primarily into particles of the hidden sector, and only a small fraction by mixing to Standard Model particles and to light H_1 pairs. The production rate of H_2, mediated by mixing, is small. In models in which the H_2 decay channels to the hidden sector are shut, H_2 will decay to SM particles with characteristics quite distinct from H_1 decays as the invariant masses of the decay final states will be different for H_1 and H_2. H_1 bosons in turn will not decay in such scenarios into novel invisible channels and decays through fluctuations to virtual H_2 states back to the Standard Model are doubly suppressed. Therefore we will focus on the light Higgs boson H_1 with properties closely related to the Standard Model[1].

All H_1 couplings to Standard Model particles are universally suppressed by the mixing parameter $\cos\chi$. In addition, H_1 may decay invisibly into the hidden sector. These two features imply

$$\begin{aligned} \sigma &= \cos^2\chi\, \sigma^{\text{SM}} \\ \Gamma_{\text{vis}} &= \cos^2\chi\, \Gamma_{\text{vis}}^{\text{SM}} \\ \Gamma_{\text{inv}} &= \cos^2\chi\, \Gamma_{\text{inv}}^{\text{SM}} + \Gamma_{\text{hid}} \ . \end{aligned} \tag{7}$$

The two parameters $\cos\chi$ and Γ_{hid} will be determined in our LHC analysis. $\Gamma_{\text{inv}}^{\text{SM}}$ is generated by Higgs decays $H \to ZZ \to 4\nu$ with an invisible Z branching ratio of 4%. If invisible Higgs decays will be observed, this 4ν rate can be predicted from observed decays $H \to ZZ \to 4\ell$ and can thus be subtracted from the new-physics signal. For the sake of simplicity we will omit $\Gamma_{\text{inv}}^{\text{SM}}$ from now on.

If the invisible decay channel is open, the κ parameter in the twin ratio Eq.(1) reads in terms of the parameters $\cos\chi$ and BR_{inv} [as generated by Γ_{hid}]:

$$\kappa = \frac{\cos^2\chi}{1+\mathcal{B}_{\text{inv}}} \leq 1 \quad \text{with} \quad \mathcal{B}_{\text{inv}} = \frac{\text{BR}_{\text{inv}}}{\text{BR}_{\text{vis}}} = \frac{\text{BR}_{\text{inv}}}{1-\text{BR}_{\text{inv}}} . \tag{8}$$

$\mathcal{B}_{\text{inv}}$ can also be expressed as the ratio of invisible decays to just one visible decay channel d, $\mathcal{B}_{\text{inv}} = \text{BR}_{\text{inv}}/(\text{BR}_d/\text{BR}_d^{\text{SM}})$. It can thus be observed without explicit reference to the total width. For $\sin\chi \ll 1$ $\mathcal{B}_{\text{inv}}$ simply approaches BR_{inv}.

---

[1] Comprehensive analyses of the H_2 boson are presently in progress.

For the Higgs portal the parameters κ and $\mathcal{B}_{\rm inv}$ are independent of the analysis channels. As a result, ratios of visible branching ratios are not modified $\text{BR}_{d_1}/\text{BR}_{d_2} = (\text{BR}_{d_1}/\text{BR}_{d_2})^{\rm SM}$. The observation of these identities provides a necessary consistency test for the hidden Higgs scenario.

The detailed experimental analysis of such a scenario will proceed in two steps: First, as long as only κ is measured but invisible Higgs decays are not, upper bounds on the mixing and, in parallel, on the fraction of invisible H_1 decays can be established,

$$\sin^2\chi \leq 1-\kappa \quad \text{and} \quad \text{BR}_{\rm inv} \leq 1-\kappa\,, \tag{9}$$

constraining the potential impact of the hidden sector on the properties of the SM-type Higgs boson. With κ measured, the hidden H_1 partial width will be correlated with the mixing parameter

$$\frac{\Gamma_{\rm hid}}{\Gamma_{\rm tot}^{\rm SM}} = \cos^2\chi\left(\frac{\cos^2\chi}{\kappa}-1\right)\,, \tag{10}$$

as illustrated in Figure 1 for $\kappa = 4/9$. For illustration purposes, the error on κ in this figure is chosen to be 10%.

Even though $\mathcal{B}_{\rm inv}$ can be in principle be determined experimentally, precise measurements of the invisible decay mode are difficult at the LHC. To show the correlation of the two parameters with the two observables we choose $\mathcal{B}_{\rm inv} = 0.5$ with a relative error of 30%, as expected for the final integrated luminosity of 300 fb^{-1} [18–21]. Combining Eq.(10) with the definition Eq.(8),

$$\frac{\Gamma_{\rm hid}}{\Gamma_{\rm tot}^{\rm SM}} = \cos^2\chi\,\mathcal{B}_{\rm inv}\,, \tag{11}$$

allows us to determine both the mixing parameter $\cos\chi$ and the H_1 partial width to the hidden sector $\Gamma_{\rm hid}$ individually, *cf.* Figure 1:

$$\cos^2\chi = \frac{\kappa}{1-\text{BR}_{\rm inv}} \qquad \text{and} \qquad \frac{\Gamma_{\rm hid}}{\Gamma_{\rm tot}^{\rm SM}} = \frac{\kappa\,\text{BR}_{\rm inv}}{(1-\text{BR}_{\rm inv})^2}\,. \tag{12}$$

The bands around the intersection point and their projections on the axes indicate the 95% CL for the parameters $\cos^2\chi$ and $\Gamma_{\rm hid}$.

In a Higgs sector likelihood analysis we can ask three kinds of questions:

1. Can we determine a non-zero mixing $\kappa \neq 1$ from a sizable Higgs sample at all?
2. To shut a Higgs portal, what size of κ can we exclude if we observe Standard Model couplings within given experimental and theory errors?
3. To verify the Higgs portal, which finite values of κ can we establish as a deviation from the Standard Model within errors. How do invisible Higgs decays affect this measurement?

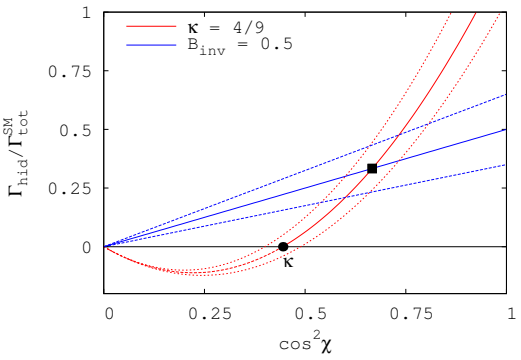

Figure 1: Correlations between $\Gamma_{\rm hid}$ and $\cos^2\chi$ as defined in Eqs.(7), based on measuring κ and $\mathcal{B}_{\rm inv}$. The two parameters are set to $\kappa = 4/9$ and $\mathcal{B}_{\rm inv} = 0.5$, respectively, for illustration. The square marks the final solution of $\cos^2\chi = 2/3$ and $\Gamma_{\rm hid}/\Gamma_{\rm tot}^{\rm SM} = 1/3$ for this parameter set. The estimated 95% CL error bands are explained in the text.

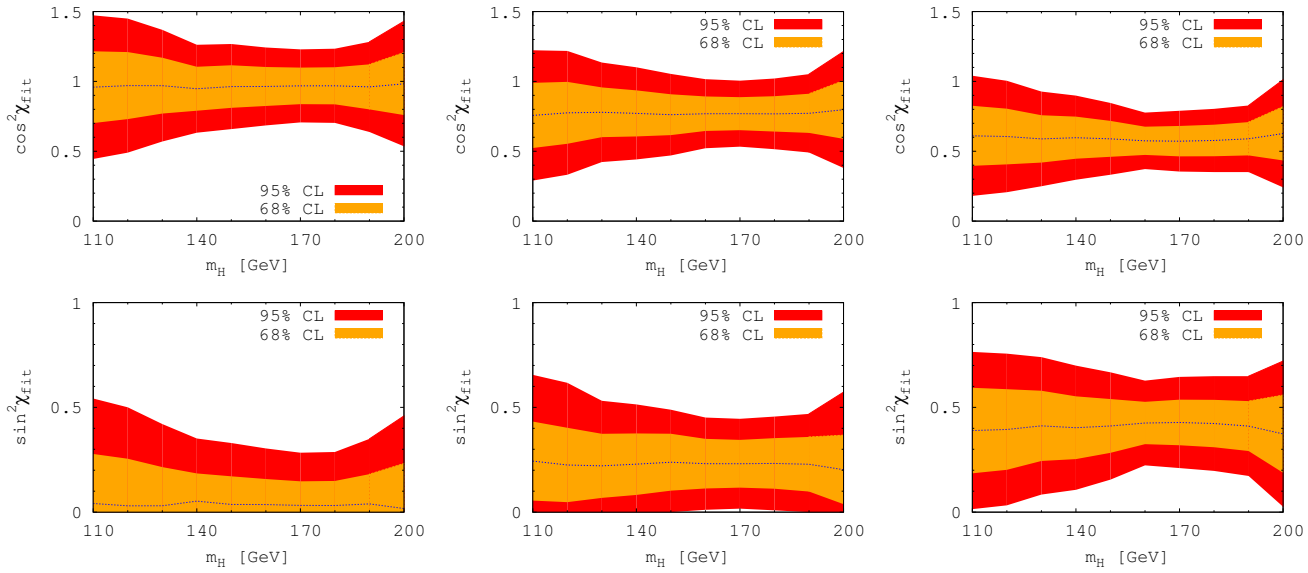

Figure 2: LHC sensitivity to modified Higgs couplings and no invisible decays $\Gamma_{\text{hid}} = 0$, based on 30 fb^{-1} of data. Upper: measurement errors as a function of the Higgs mass for $\cos^2\chi_{\text{th}} = 1.0$ [left], $\cos^2\chi_{\text{th}} = 0.8$ [center] and $\cos^2\chi_{\text{th}} = 0.6$ [right]. Lower: resulting upper and lower bounds on the mixing parameter $\sin^2\chi$, constrained to the physical range.

To answer the first question, the upper panels in Figure 2 show the bounds on $\kappa = \cos^2\chi$ which we can set by analyzing a sample of Standard Model Higgs bosons with masses between 110 and 200 GeV. Invisible Higgs decays we neglect in this first step, but all standard Higgs search channels are exploited based on an integrated luminosity of 30 fb^{-1} [4]. Starting with the Standard Model hypothesis at $m_H = 120$ GeV we can measure $\cos^2\chi = 1 \pm 24\%(48\%)$ at the $68\%(95\%)$ CL. For larger Higgs masses the error bar improves by a factor of two, due to an increased statistics of the comparably clean WW and ZZ channels. For even larger Higgs masses around 200 GeV the over-all event rate drops again, increasing the measurement error again. As shown in the lower panels of Figure 2 we can also translate the minimal values of κ into maximal values of the mixing parameter $\sin^2\chi$ according to Eq.(9). In contrast to the upper limits on $\cos^2\chi$ the limits on $\sin^2\chi$ include the constraint $0 \leq \sin^2\chi \leq 1$. In Table I we collect the bounds on a modified Higgs coupling, including the constraint, for three Higgs masses, based on an integrated luminosity of 30 fb^{-1} as well as expectations for an integrated luminosity of 300 fb^{-1}. Even without observing invisible decays explicitly, we can translate these results into upper bounds on the invisible decay width according to Eq.(8). These bounds are shown in the right column of the table.

The error on the scaled Higgs couplings includes another square root, which translates into a relative error $(\Delta g)/g \sim 10\%(20\%)$. These limits measure how well the Higgs mechanism in the Standard Model can be established quantitatively, and they have to be compared to an independent variation of all Higgs couplings, which for $m_H = 120$ GeV are expected to be measured to $\mathcal{O}(25\% - 50\%)$ [4]. The sizable improvement of the constrained analysis arises first of all because all experimental channels now contribute to the same measurement, and secondly because they also determine the total Higgs width much more precisely than the $H \to b\bar{b}$ fat-jet analysis.

Before moving away from Standard Model decays only, we show the results of a two-parameter fit in the upper panels of Figure 3, while keeping $\Gamma_{hid} = 0$. Compared to the one-dimensional parameter extraction shown in Figure 2 the error on the extracted value of $\cos^2\chi$ is now increased. This arises because we now have to perform a two-dimensional parameter extraction and project the correlated uncertainty onto the two model parameters $\cos\chi$ and Γ_{hid}. Comparing the upper panels of Figure 3 to Figure 2 shows this effect on the extracted parameters, just fitting two parameters without even introducing an invisible Higgs decay. The error on $\cos^2\chi$ becomes asymmetric due to the positivity constraint on the Higgs width, fixing the upper error band of $\cos^2\chi$. On the other hand, fake invisible-decay events from background fluctuations lead to a wide lower error bound.

M_H [GeV]	$\kappa >$		$\sin^2\chi, \text{BR}_{\text{inv}} <$		$\Gamma_{\text{hid}}/\Gamma^{\text{SM}}_{\text{tot}} <$	
120	0.50	0.76	0.50	0.24	1.0	0.32
160	0.70	0.82	0.30	0.18	0.43	0.22
200	0.54	0.73	0.46	0.27	0.85	0.37

Table I: Upper bounds [95% CL] on mixing and invisible decays expected to be set in a Higgs sample within the Standard Model for integrated luminosities of 30 [left] and 300 fb^{-1} [right].

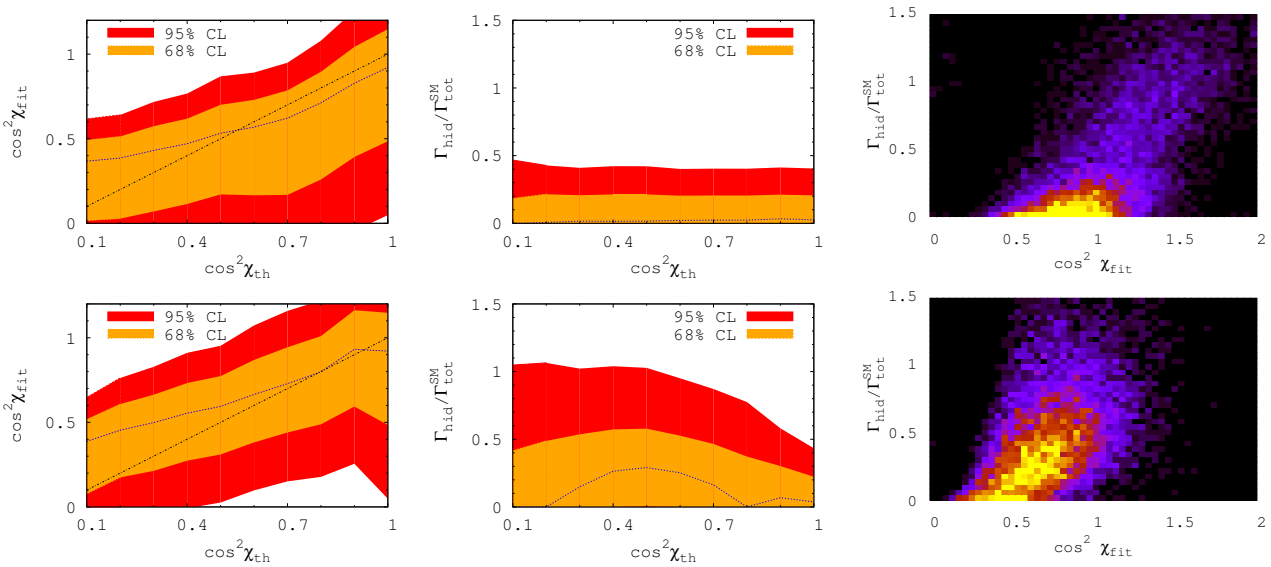

Figure 3: LHC sensitivity to modified Higgs couplings and invisible decays, based on 30 fb^{-1} of data. Upper row: $\Gamma_{\text{hid}} = 0$; lower row $\Gamma_{\text{hid}} = \sin^2\chi\,\Gamma^{\text{SM}}_{\text{tot}}$ for invisible decays. The Higgs mass is fixed to 120 GeV. Left column: extracted $\cos^2\chi_{\text{fit}}$ values as a function of $\cos^2\chi_{\text{th}}$; Center column: extracted bounds and measurements of $\Gamma_{\text{hid}}/\Gamma^{\text{SM}}_{\text{tot}}$ as a function of $\cos^2\chi_{\text{th}}$; Right column: illustration of the correlation between mixing and invisible partial width using $\cos^2\chi_{\text{th}} = 1.0$ [upper row] and 0.6 [lower row].

Moreover, we observe a clear bias towards too large event numbers towards small values of $\cos^2\chi$. This is in part due to the asymmetric Poisson distribution and in part due to the fact that measurement channels where the number of background events from the control region exceeds the number of events in the signal region, are explicitly excluded from the fit. A more detailed discussion of this effect is presented in Appendix A. Finally, the error band for the extracted Γ_{hid} ranges around 20% of the Standard Model width.

The impact of actual invisible decays is estimated by choosing $\Gamma_{\text{hid}} = \sin^2\chi\,\Gamma^{\text{SM}}_{\text{tot}}$ as illustrative example for the parametrization of the non-zero invisible partial width. This parametrization accounts naturally for the suppression of Γ_{hid} by mixing, while a coefficient of size $\Gamma^{\text{SM}}_{\text{tot}}$ would be expected for structures in the hidden sector roughly parallel to the standard sector [5]. Comparing the upper and lower left panels of Figure 3, it is evident that the effect of an actual invisible Higgs decay on the extraction of $\cos^2\chi$ is small. A measurement of the invisible Higgs width, beyond setting upper bounds, seems challenging with only 30 fb^{-1} of integrated luminosity. The best discrimination power we obtain for medium-sized values of $\cos^2\chi$, where we have a significant invisible branching ratio and the production side is not strongly suppressed.

Finally, in the right panels we see a clear correlation between the two extracted parameters, owed to the form of the observables shown in Eq.(8) and Figure 1.

III. STRONGLY INTERACTING HIGGS BOSON

Deviations of the Higgs couplings similar to the $\cos\chi$ factor in Eq.(7) are expected when a light Higgs boson is generated as a pseudo-Goldstone boson by global symmetry breaking in a new strong interaction sector. Depending on the details of the model, the Higgs couplings are modified either individually for different particle species, or universally for all species [10–12]. In contrast to the hidden Higgs model, the light Higgs boson H_1 does not decay into channels not present in the Standard Model.

Such a picture can be developed using Holographic Higgs Models, based on the AdS/CFT correspondence, in which strongly coupled theories in four dimensions are identified with weakly coupled theories in five dimensions [30]. For example, the spontaneous breaking of a global symmetry $SO(5) \to SO(4)$ generates the adequate iso-doublet of Goldstone bosons. Assigning the Standard Model fermions either to spinorial or fundamental $SO(5)$ representations changes the Higgs couplings either

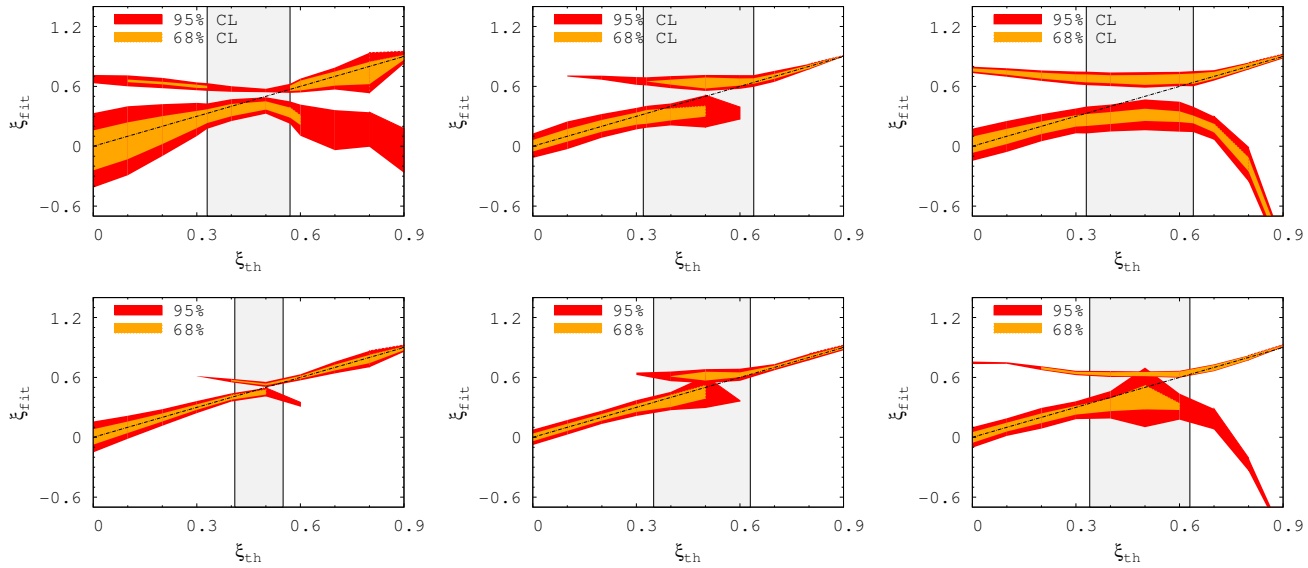

Figure 4: LHC sensitivity to modified Higgs couplings based on 30 [upper] and 300 fb^{-1} [lower row] for un-aligned boson and fermion couplings as a function of the assumed $\xi_{\rm th}$ for $m_H = 120$ GeV (left), 160 GeV (center) and 200 GeV (right). ξ values close to 1/2, for which the rates are strongly suppressed, are blinded by the gray bars.

universally or separately for Standard Model vectors and fermions[2]. The modifications are determined by the parameter

$$\xi = \left(\frac{v}{f}\right)^2 \tag{13}$$

which measures the magnitude of the Goldstone scale f in relation to the standard Higgs vacuum expectation value v. The case where all Higgs couplings are suppressed universally by a factor $(1-\xi)^{1/2}$, is covered by the analysis in the preceding section identifying

$$\kappa \equiv 1 - \xi\,. \tag{14}$$

All results from the Higgs portal can be transferred one-by-one to this universal strong interaction model, identifying $\cos^2\chi \to 1-\xi$ and setting $\mathcal{B}_{\rm inv} = 0$. Hence, it can be concluded from Figure 2 that ξ can be measured with an uncertainty of $10\% - 20\%$, depending on the Higgs mass.

In a closely related scenario [12] universality is broken to the extent that the Higgs coupling of vector particles is reduced, still, by $(1-\xi)^{1/2} \approx 1-\xi/2$ but the coupling of fermions by a different coefficient, $(1-2\xi)/(1-\xi)^{1/2} \approx 1-3\xi/2$. Now, the two κ parameters of the twin width-ratios, at small ξ, read

$$\begin{aligned} \kappa_V &= 1 - \left[1(3) - 2\,{\rm BR}_{\rm f}^{\rm SM}\right]\,\xi \\ \kappa_f &= 1 - \left[3(5) - 2\,{\rm BR}_{\rm f}^{\rm SM}\right]\,\xi\,, \end{aligned} \tag{15}$$

The indices V, f distinguish vector and fermion Higgs decays, and the expression in brackets corresponds to production either in Higgs-strahlung/electroweak boson fusion or — altered to () — in gluon fusion; ${\rm BR}_{\rm f}^{\rm SM}$ denotes the inclusive Higgs branching ratio to fermions in the Standard Model which is close to one for light Higgs bosons.

The two κ parameters of this non-universal strong interaction model are characteristically different from both the universal strong interaction model as well as the Higgs portal. First, they are different for vector and fermion decays of the Higgs particle; second, in parameter regions in which more than half of the Higgs decays are fermionic, κ_V is larger than unity for Higgs-strahlung/electroweak fusion.

---

[2] With f larger than v, the mass scale of the new fields in such scenarios will be about 1 TeV and above. Their effect on Higgs couplings to SM fields through loops will therefore, quantum mechanically, be strongly suppressed. Though the normal SM modes are largely decoupled near $\xi = \frac{1}{2}$, *cf.* Appendix B, the overall coupling mediated by the new fields will remain small and the production of the Higgs particles in the parameter range will correspondingly be suppressed. In fact, this parameter range must be blinded in our analysis as a result, *cf.* Figure 4

		30 fb^{-1}						300 fb^{-1}					
M_H [GeV]	ξ_{th}	ξ_1	$\Delta\xi_1$	w_{ξ_1}	ξ_2	$\Delta\xi_2$	w_{ξ_2}	ξ_1	$\Delta\xi_1$	w_{ξ_1}	ξ_2	$\Delta\xi_2$	w_{ξ_2}
120	0.0	-0.04	0.36	0.94	0.67	0.06	0.06	0.0	0.14	0.99	0.67	0.08	0.01
	0.2	0.16	0.26	0.88	0.63	0.06	0.12	0.20	0.08	0.99	0.63	0.02	0.01
	0.6	0.61	0.06	0.54	0.26	0.18	0.46	0.60	0.02	0.96	0.31	0.04	0.04
160	0.0	0.0	0.12	0.98	0.73	0.03	0.02	0.0	0.08	1.0	—	—	0
	0.2	0.20	0.10	0.95	0.69	0.04	0.05	0.20	0.08	0.99	0.67	0.04	0.01
	0.6	0.64	0.06	0.85	0.33	0.10	0.15	0.63	0.04	0.96	0.36	0.08	0.04
200	0.0	0.01	0.16	0.84	0.77	0.03	0.16	0.0	0.10	0.92	0.75	0.014	0.08
	0.2	0.19	0.14	0.67	0.71	0.04	0.33	0.19	0.10	0.79	0.69	0.018	0.21
	0.6	0.67	0.06	0.50	0.30	0.16	0.50	0.63	0.03	0.55	0.31	0.16	0.45

Table II: Errors $\Delta\xi$ [95% CL] on the pseudo-Goldstone parameter ξ for integrated luminosities of 30 [left] and 300 fb^{-1} [right]. Shown are the two solutions together with their corresponding probability w_ξ of the best-fit, which are the relative numbers of toy experiments ending up in the vicinity [as obtained by a fit of two Gauss peaks] of this solution.

Results for this model are presented in Figure 4 and in Table II for 30 and 300 fb^{-1}. At low luminosity two solutions emerge, while an increased luminosity eliminates the fake solution in major parts of the parameter space, as long as the Higgs mass is small. The mathematical evolution of the two solutions and their analytical form is discussed in Appendix B. Around $\xi \sim 0.5$ the observable rates at the LHC drop sharply, not allowing for a reliable extraction of ξ simply based on too little statistics for the fit. Therefore, the gray bands blind ranges of parameter space in which the modified theory leads to too large a suppression. Only when our fit finds $\chi^2/\text{d.o.f} \gtrsim 1$ the result becomes statistically trustworthy again.

In contrast to 120 GeV, we observe that the situation hardly improves for a 200 GeV Higgs boson once we go to higher luminosity. For this mass only four Higgs channels are left. All include a decay into either W or Z bosons, and on the production side three of them are proportional to g_{ttH}, either via gluon-fusion or top-quark associated production. These three measurements are equivalent and exhibit an ambiguity because fermion-Higgs couplings cannot distinguish between small and large values of ξ, see Appendix B. Only the fourth measurement based on weak-boson fusion production can resolve the ambiguity. Even though this channel is comparably clean, it is systematics limited, *i.e.* it hardly improves with higher luminosities.

Also we need to establish that the couplings indeed follow this pattern. To quantify this we perform a fit of vector and fermion couplings separately, illustrated in Fig. 5 using theory scenarios for $\xi_{\text{th}} = 0$ (SM), 0.2 and 0.6 with a luminosity of 30 fb^{-1}. We find for the SM case that we can determine the vector couplings with a 2σ error of 0.22 and the fermion couplings with an accuracy of 0.55. A positive correlation between the two parameters of 0.59, which is approximately aligned with the model prediction as function of ξ, further improves our possibility to exclude deviations. The 95% CL region intersects the theory line at $\xi = -0.38$ and 0.24. For $\xi_{\text{th}} = 0.2$ the changes are small, with a slightly improved precision on the fermionic couplings and a larger correlation. In the $\xi_{\text{th}} = 0.6$ case the fake solution around smaller ξ values is again similar, while the correct one yields a different behavior. The correlation has changed sign, making it more difficult to discern it from other models which do not follow the distinct pattern. As two standard deviation errors we obtain smaller values for this solution on the other hand. They are 0.16 and 0.20 for fermion and vector couplings, respectively.

The two solutions shown in Figure 4 also represent a technical challenge. We need to know not only the error $\Delta\xi$ on the individual solution, but also the probability w_ξ with which this solution appears. A Minuit fit per toy-experiment alone cannot achieve this, because there is no guarantee that it will find the global minimum of χ^2. Indeed, we observe a strong dependence on the starting point in Minuit. Therefore, we need to add a coarse grid scan of the one-dimensional parameter space before the minimization. To obtain the 68% and 95% confidence levels in Figure 4 we first fit a sum of two Gaussians to the parameter distribution. To extract a confidence level interval around each of the two peaks we define a height which crosses both Gaussians such that the sum of the two central areas corresponds to 68% or 95% of the entire integral under both Gaussians. The two intersections of this horizontal line with each Gaussian give us the confidence regions quoted for example in Figure 4.

First of all, in Figure 4 we again see that the typical error bars shrink when we increase the Higgs mass and with it the number of events from 120 GeV to 160 GeV. For even larger Higgs masses some of the relevant channels rapidly vanish, so the error bars increase again. The actual error bars for the different scenarios are listed in Table II. In particular for moderate luminosity the absolute error on ξ_1, for assumed values of $\xi_{\text{th}} < 0.2$ range around 20% for a light Higgs boson and well below 10% towards larger mass. These numbers again roughly compare to the typical values for $\Delta\xi$ in the universal strongly interacting model or $\sqrt{\Delta\kappa}$ for the Higgs portal. For larger values of $\xi \geq 0.6$ the two strongly interacting models start deviating significantly. In particular, the relative error $\Delta\xi_1/\xi_1$ decreases dramatically. The reason will be discussed in detail in Appendix B: due to the non-universal structure of the fermion and vector couplings in this range the Higgs event rates vary much more strongly than elsewhere. Therefore, the LHC will probe this region with high precision, with the slight caveat that towards slightly smaller ξ the Higgs production and decay rates vanish rapidly. These are precisely the dangerous gray regions in Figure 4 — as long as we observe Higgs events at the LHC the sharp drop in rates towards $\xi = 0.5$ is a welcome feature to analyze the model at colliders.

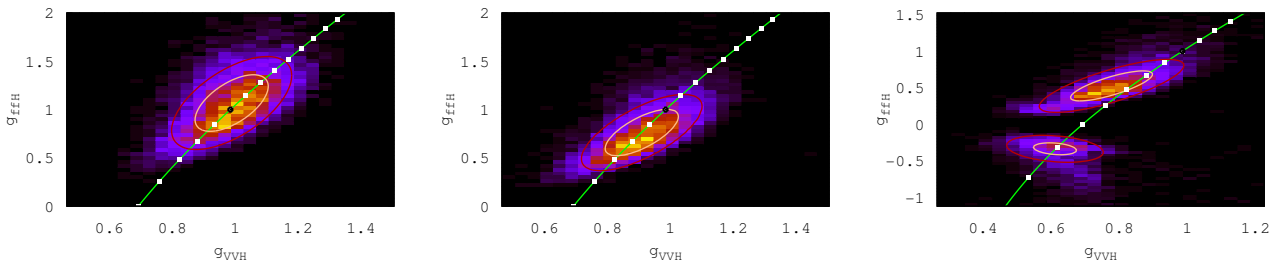

Figure 5: Independent fit of common vector [g_{VVH}] and fermion [g_{ffH}] Higgs couplings for $\xi_{\text{th}} = 0$, 0.2 and 0.6 using 30 fb^{-1}. The ξ values correspond to $g_{VVH} = 1$, 0.89, 0.63 and $g_{ffH} = 1$, 0.67, -0.32, respectively. The red and orange ellipses show the 68% and 95% CL regions. The green line marks the model prediction, with the black dot indicating $\xi = 0$ and the white dots in 0.1 distance, moving to positive values towards the lower left.

The improvement of the errors with increased statistics is also shown in Table II. If the measurement were statistics dominated, the error would be reduced by a factor $\sqrt{10} \simeq 3$ when going from 30 to 300 fb^{-1}. From the results we find that the improvement is smaller. The reason is that all measurements determine only a single parameter, so unlike in the unconstrained Higgs sector analysis [4] in the current setup even for 30 fb^{-1} the results are not entirely statistics dominated.

IV. SUMMARY

In this letter we have analyzed the LHC reach for deviations of Higgs couplings from their Standard Model values. Two models can be linked to such signatures: First, we couple the Standard Model Higgs field to a hidden Higgs sector, opening a renormalizable Higgs portal between the two sectors. From the event rates for visible Higgs production and decay channels we could derive upper bounds on non-SM admixtures in the wave-function of the Higgs boson and on novel invisible decay channels. Since it is unclear if at the LHC we will be able to quantitatively analyze invisible Higgs decays, given the experimental errors, the question arises if we include the invisible Higgs decay rate in a two-dimensional fit or only include modified visible couplings.

From the two-dimensional fit we find 95% CL limits on the two model parameters $\sin^2\chi < 0.50$ and $\Gamma_{\text{hid}}/\Gamma^{\text{SM}}_{\text{tot}} < 1.0$ ($\mathcal{L} = 30\,\text{fb}^{-1}$ and $m_H = 120\,\text{GeV}$). Towards Higgs masses around 160 GeV these limits slightly improve, while for even heavier masses the decreasing production rates at the LHC take their toll. These numbers correspond to a 10% to 20% measurement of the modified Higgs couplings $(\Delta g)/g$. Such bounds also quantify to what accuracy a Higgs boson discovered and studied at the LHC could be identified as the Standard Model realization. They should be compared to limits on the individual Higgs couplings from general Higgs sector analyses [3, 4] and they show a significant improvement driven by the higher level of specification in the hypothesis tested.

Neglecting the invisible Higgs decay and hence trading the minimal amount of extra information for the advantage of a one-dimensional fit without additional noise in a small region of parameter space ($m_H \sim 160$ GeV and $\cos^2\chi \sim 0.6$) we might even be able to establish a Higgs portal at the 5σ level based on an integrated luminosity of 30 fb^{-1}.

If invisible decay channels of the Higgs boson are indeed measured, the mixing parameter and the partial width for Higgs decays to the hidden sector can of course be determined individually. However, such a measurement will likely require higher luminosities.

A related problem arises when a light Higgs boson is identified with a pseudo-Goldstone boson associated with the spontaneous breaking of global symmetries in new strong interactions. If fermion and vector couplings are scaled equally, the scaling analysis of the hidden sector can be transcribed without change, assuming there are no Higgs decays into non-SM channels. The bound on $\sin^2\chi$ can simply be read as a bound on ξ.

More interestingly, if the Higgs couplings are modified separately for vectors and fermions, various production/decay channels may be analyzed individually so that a unique picture emerges. For small values of ξ the two kinds of couplings at least qualitatively scale similarly, so our results for $(\Delta\xi)/\xi$ follow the usual patterns. For larger values around $\xi \sim 0.5$ the Higgs-fermion couplings now vanish, leading to wells in the Higgs event rates. In those regions the relative error on the determination of ξ can shrink to 5%, though being dangerously close to parameter regions where the Higgs discovery would require larger LHC luminosities.

The LHC will be able to probe scenarios with modified Higgs couplings as generally analyzed in Refs. [3, 4]. However, testing a specific one- or two-parameter model appears to be a promising strategy to gain insight into the Higgs sector already based on an integrated luminosity of 30 fb^{-1} at 14 TeV. Compared to the general analysis the typical error bars on Higgs couplings are reduced by at least a factor $1/2$, now ranging around 10% to 20% for Higgs masses between 120 GeV and 200 GeV.

Acknowledgments

PMZ is grateful to the Institut für Theoretische Teilchenphysik und Kosmologie for the warm hospitality extended to him at RWTH Aachen University. MR acknowledges support by the Deutsche Forschungsgemeinschaft via the Sonderforschungsbereich/Transregio SFB/TR-9 'Computational Particle Physics' and the Initiative and Networking Fund of the Helmholtz Association, contract HA-101 (Physics at the Terascale). MR, DZ and PMZ are grateful to the Institut für Theoretische Physik of Heidelberg University for the hospitality. Part of the work by DZ is supported by the GDR Terascale of the CNRS.

Appendix A: Observational bias

Statistical fluctuations in the measurements can lead to situations which cannot be interpreted in terms of physically meaningful parameters. One such example is a negative number of signal events. At the LHC we first measure the sum of signal and background events in the signal region. The number of background events we then determine either from extrapolation from a signal-free control region, like sidebands, or from Monte Carlo simulations. The difference gives us the number of signal events. At arbitrarily large statistical significances the difference between the two measurements, *i.e.* the number of signal events, is by definition much larger than the statistical error on each of them individually. However, for significances between one and three standard deviations as we expect them for the Higgs sector at the LHC a downward fluctuation in signal-plus-background and an upward fluctuation in background-only can lead to a negative difference. This effect has to be dealt with when we compose the sample of measurements which for example enter the Higgs sector analysis presented in this paper. The question is, if solutions to this problem will affect for example the central values and errors quoted for the Higgs couplings.

We present three alternative treatments in Figure 6. On the left-hand side we only take into account channels where we measure a positive number of signal events. This prescription we use in our analysis. For couplings fairly close to their Standard Model values we obtain the correct central value. For small couplings we observe a significant shift to larger values. The reason is that if a measurement shows an upward signal fluctuation we include it, while a downward fluctuation quickly reaches the negative-S threshold and gets excluded.

In the central panel we only include measurements where the nominal number of signal and background events yields a 2σ excess. We find good agreement between fitted and truth values of χ, but for $\cos^2\chi < 0.7$ there are no measurements left which fulfill this condition.

For the right panel we only include channels where the measured numbers yield a 2σ excess. Here, we observe a significant upward shift over the whole parameter range. Even for Standard Model couplings the actual Standard Model is almost excluded at the 95% CL. Therefore, it is important to take into account measurements which have a low observed significance on their own. They can provide upper bounds on Higgs couplings and avoid a bias generated by upward fluctuations of signal events in some of the channels included.

Appendix B: Scaling of cross sections in a strongly interacting Higgs scenario

For the un-aligned shifts of Higgs-gauge and Yukawa couplings the scaling of the cross sections with ξ does not follow a simple pattern. However, the main features can be illustrated for two characteristic leading channels, Higgs-strahlung $q\bar{q}' \to WH, H \to b\bar{b}$, and gluon-fusion $gg \to H \to \gamma\gamma$. Ignoring resummation effects in this qualitative discussion, the corresponding

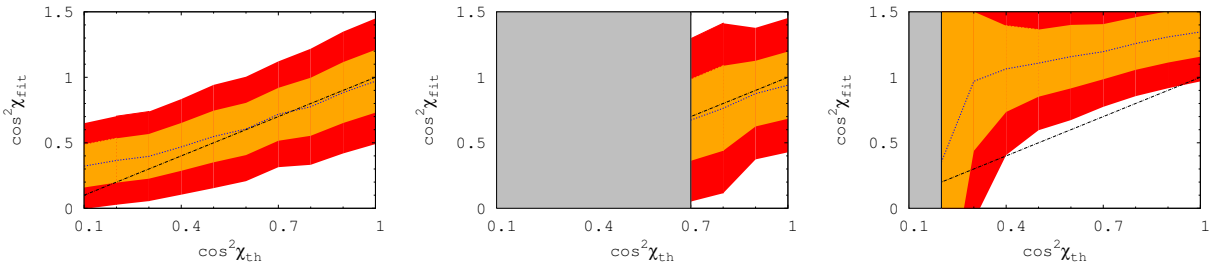

Figure 6: Different treatment of channels, depending on the number of events in the signal region $S + B$, compared to background events B from a signal-free control region. Left: a measurement is included when $S + B > B$. Center: only measurements corresponding to at least a 2σ excess for nominal signal and background rates are included. Right: only measurements for which the measured values of $S + B$ and B give at least two standard deviations are included.

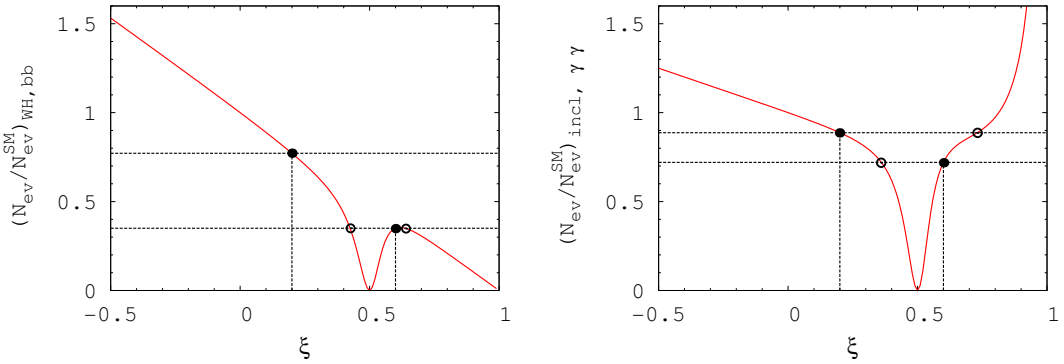

Figure 7: The scaling functions for Higgs-strahlung $WH, H \to b\bar{b}$ and gluon fusion $gg \to H \to \gamma\gamma$. The full circle on the straight lines marks the true unique solution, while the open circles denote fake values which are different for the two channels.

scaling functions, normalized to unity at the Standard Model value $\xi = 0$, can be approximated as

$$\left(\frac{N_{\rm ev}}{N_{\rm ev}^{\rm SM}}\right)_{WH,bb} = \frac{1}{\mathcal{N}_{WH,bb}} \frac{(1-\xi)\,\dfrac{(1-2\xi)^2}{(1-\xi)}}{\dfrac{(1-2\xi)^2}{(1-\xi)} + \gamma(1-\xi)}$$

$$\left(\frac{N_{\rm ev}}{N_{\rm ev}^{\rm SM}}\right)_{gg,\gamma\gamma} = \frac{1}{\mathcal{N}_{gg,\gamma\gamma}} \frac{\dfrac{(1-2\xi)^2}{(1-\xi)}\left[\dfrac{(1-2\xi)^2}{(1-\xi)} + \beta_1(1-2\xi) + \beta_2(1-\xi)\right]}{\dfrac{(1-2\xi)^2}{(1-\xi)} + \gamma(1-\xi)}\,. \tag{B1}$$

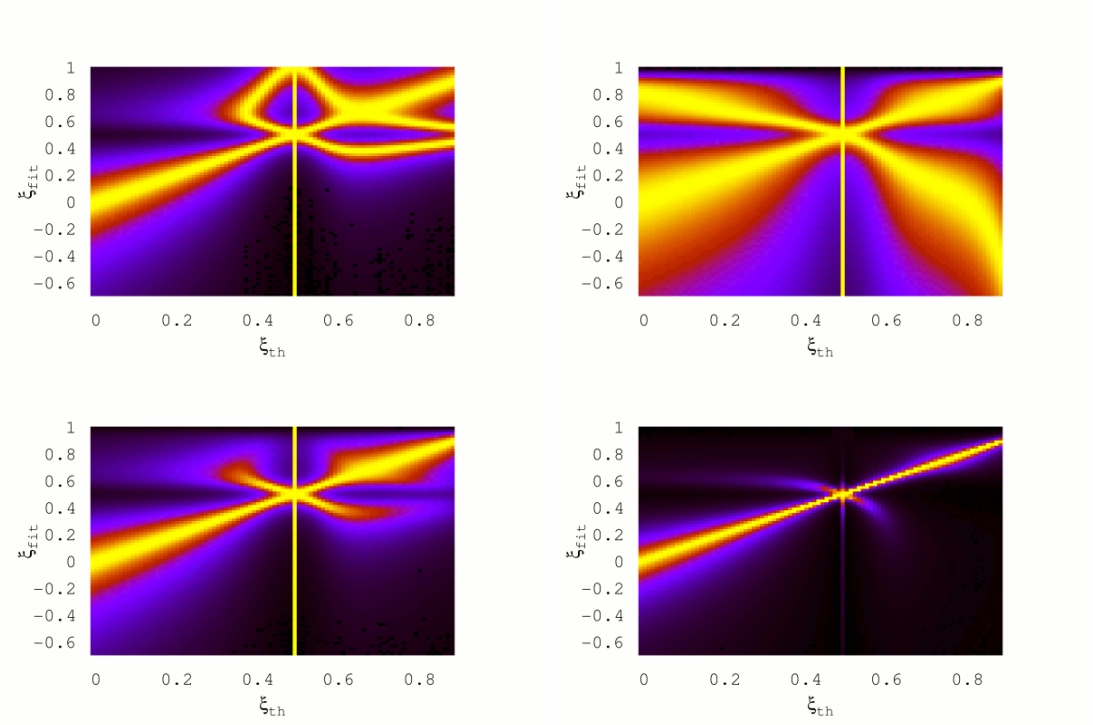

Figure 8: Extracted values for ξ as a function of the assumed $\xi_{\rm th}$ for $M_H = 120$ GeV and 30 fb^{-1}. We show profile likelihoods, where we have neglected theory errors for clarity. Upper: Higgs-strahlung plus $b\bar{b}$ decay [left], and gluon fusion plus $\gamma\gamma$ decay [right]. Lower: Combination of the two channels [left] and including all available channels [right].

The parameter $\gamma \sim 0.05$ accounts for the admixture of $H \to WW$ and ZZ decays compared to $H \to b\bar{b}$ for Higgs masses close to 120 GeV while $\beta_{1,2} \sim -8.9,\ 19.8$ parametrize top- and W-loop contributions for Higgs decays to photons, including their destructive interference.

As shown in Figure 7 the scaling function for Higgs-strahlung plus $b\bar{b}$ decays falls off straight, apart from a narrow well close to $\xi = 1/2$. There, the rates for observing a Higgs boson are driven to zero. The scaling function for gluon fusion and $\gamma\gamma$ decay behaves similarly, except above the well, where the scaling function diverges for $\xi \to 1$. The multiplicities of the solutions are illustrated for $\xi = 0.2$ and $\xi = 0.6$ by the two dashed lines. Depending on the value of ξ, either one or up to three solutions correspond to given values of the scaling functions. By combining the two sets of the solutions for the two channels the individual ambiguities are resolved: the fake solutions for ξ [open circles] are eliminated and only the true value [full circle] remains.

This theoretical picture is realized only for large event numbers. Otherwise, remnants of the fake solutions cannot be eliminated completely. This is illustrated in Figure 8 where we present the log-likelihood bands for ξ. In the upper panels we show the individual Higgs-strahlung and gluon-fusion channels, including their individual fake solutions. In the lower panels we first combine the two channels, strongly reducing the fake solutions. In the bottom right panel we include all available channels, eliminating entirely the fake solutions. Only the width around the true value in two preferred directions remains.

[1] A. Djouadi, Phys. Rept. **457**, 1 (2008); and Phys. Rept. **459**, 1 (2008).

[2] M. Spira, Fortsch. Phys. **46**, 203 (1998); V. Buescher and K. Jakobs, Int. J. Mod. Phys. A **20**, 2523 (2005); D. Rainwater, [arXiv:hep-ph/0702124]; M. Gomez-Bock, M. Mondragon, M. Muhlleitner, M. Spira and P. M. Zerwas, [arXiv:0712.2419 [hep-ph]]; J. D. Wells, [arXiv:0909.4541 [hep-ph]]; T. Plehn, [arXiv:0910.4182 [hep-ph]].

[3] M. Duhrssen, S. Heinemeyer, H. Logan, D. Rainwater, G. Weiglein and D. Zeppenfeld, Phys. Rev. D **70**, 113009 (2004).

[4] R. Lafaye, T. Plehn, M. Rauch, D. Zerwas and M. Duhrssen, JHEP **0908**, 009 (2009).

[5] R. Barbieri, T. Gregoire and L. J. Hall, arXiv:hep-ph/0509242; M. J. Strassler and K. M. Zurek, Phys. Lett. B **651**, 374 (2007); B. Patt and F. Wilczek, arXiv:hep-ph/0605188; M. J. Strassler and K. M. Zurek, Phys. Lett. B **661**, 263 (2008).

[6] M. Bowen, Y. Cui and J. D. Wells, JHEP **0703** (2007) 036; V. Barger, P. Langacker, M. McCaskey, M. J. Ramsey-Musolf and G. Shaughnessy, Phys. Rev. D **77**, 035005 (2008).

[7] T. Binoth and J. J. van der Bij, Z. Phys. C **75**, 17 (1997)

[8] D. E. Morrissey, T. Plehn and T. M. P. Tait, arXiv:0912.3259 [hep-ph].

[9] D. B. Kaplan, H. Georgi and S. Dimopoulos, Phys. Lett. B **136**, 187 (1984); H. Georgi and D. B. Kaplan, Phys. Lett. B **145**, 216 (1984); H. Georgi, D. B. Kaplan and P. Galison, Phys. Lett. B **143**, 152 (1984).

[10] G. F. Giudice, C. Grojean, A. Pomarol and R. Rattazzi, JHEP **0706**, 045 (2007); I. Low, R. Rattazzi and A. Vichi, JHEP **1004**, 126 (2010).

[11] T. Han, D. Krohn, L. T. Wang and W. Zhu, JHEP **1003**, 082 (2010); R. Contino, C. Grojean, M. Moretti, F. Piccinini and R. Rattazzi, JHEP **1005**, 089 (2010).

[12] J. R. Espinosa, C. Grojean and M. Muhlleitner, JHEP **1005**, 065 (2010).

[13] W. Buchmuller and D. Wyler, Nucl. Phys. B **268**, 621 (1986); K. Hagiwara, R. Szalapski and D. Zeppenfeld, Phys. Lett. B **318**, 155 (1993).

[14] T. Plehn, D. L. Rainwater and D. Zeppenfeld, Phys. Rev. Lett. **88**, 051801 (2002); V. Hankele, G. Klamke, D. Zeppenfeld and T. Figy, Phys. Rev. D **74**, 095001 (2006); C. Ruwiedel, N. Wermes and M. Schumacher, Eur. Phys. J. C **51**, 385 (2007).

[15] J. R. Dell'Aquila and C. A. Nelson, Phys. Rev. D **33**, 80 (1986); C. A. Nelson, Phys. Rev. D **37**, 1220 (1988); B. Field, Phys. Rev. D **66**, 114007 (2002); D. J. . Miller, S. Y. Choi, B. Eberle, M. M. Muhlleitner and P. M. Zerwas, Phys. Lett. B **505**, 149 (2001); S. Y. Choi, D. J. . Miller, M. M. Muhlleitner and P. M. Zerwas, Phys. Lett. B **553**, 61 (2003); Y. Gao, A. V. Gritsan, Z. Guo, K. Melnikov, M. Schulze and N. V. Tran, Phys. Rev. D **81**, 075022 (2010); A. De Rujula, J. Lykken, M. Pierini, C. Rogan and M. Spiropulu, arXiv:1001.5300 [hep-ph].

[16] K. Hagiwara, P. Konar, Q. Li, K. Mawatari and D. Zeppenfeld, JHEP **0804**, 019 (2008); K. Hagiwara, J. Kanzaki, Q. Li and K. Mawatari, Eur. Phys. J. C **56**, 435 (2008).

[17] V. Barger, T. Han, P. Langacker, B. McElrath and P. Zerwas, Phys. Rev. D **67**, 115001 (2003).

[18] O. J. P. Eboli and D. Zeppenfeld, Phys. Lett. B **495**, 147 (2000); R. M. Godbole, M. Guchait, K. Mazumdar, S. Moretti and D. P. Roy, Phys. Lett. B **571**, 184 (2003).

[19] G. Aad *et al.* [The ATLAS Collaboration], arXiv:0901.0512 [hep-ex].

[20] G. L. Bayatian *et al.* [CMS Collaboration], J. Phys. G **34**, 995 (2007).

[21] A. De Roeck *et al.*, Eur. Phys. J. C **66**, 525 (2010).

[22] J. M. Butterworth, A. R. Davison, M. Rubin and G. P. Salam, Phys. Rev. Lett. **100**, 242001 (2008); T. Plehn, G. P. Salam and M. Spannowsky, Phys. Rev. Lett. **104**, 111801 (2010).

[23] The ATLAS Collaboration, ATL-PHYS-PUB-2009-088 (2009).

[24] A. Djouadi, M. Spira and P. M. Zerwas, Phys. Lett. B **264** (1991) 440; S. Dawson, Nucl. Phys. B **359** (1991) 283; M. Spira, A. Djouadi, D. Graudenz and P. M. Zerwas, Nucl. Phys. B **453** (1995) 17; R. V. Harlander and W. B. Kilgore, Phys. Rev. Lett. **88**, 201801 (2002); C. Anastasiou and K. Melnikov, Nucl. Phys. B **646**, 220 (2002); V. Ravindran, J. Smith and W. L. van Neerven, Nucl. Phys. B **665**,

325 (2003); S. Moch and A. Vogt, Phys. Lett. B **631**, 48 (2005); A. Pak, M. Rogal and M. Steinhauser, JHEP **1002**, 025 (2010); R. V. Harlander, H. Mantler, S. Marzani and K. J. Ozeren, Eur. Phys. J. C **66**, 359 (2010).

[25] T. Han, G. Valencia and S. Willenbrock, Phys. Rev. Lett. **69**, 3274 (1992); T. Figy, C. Oleari and D. Zeppenfeld, Phys. Rev. D **68**, 073005 (2003); M. Ciccolini, A. Denner and S. Dittmaier, Phys. Rev. Lett. **99**, 161803 (2007). and Phys. Rev. D **77**, 013002 (2008); K. Arnold *et al.*, Comput. Phys. Commun. **180**, 1661 (2009); P. Bolzoni, F. Maltoni, S. O. Moch and M. Zaro, Phys. Rev. Lett. **105**, 011801 (2010).

[26] A. Djouadi, M. Spira and P. M. Zerwas, Z. Phys. C **70**, 427 (1996).

[27] A. Djouadi, J. Kalinowski and M. Spira, Comput. Phys. Commun. **108**, 56 (1998).

[28] A. Hocker, H. Lacker, S. Laplace and F. Le Diberder, Eur. Phys. J. C **21**, 225 (2001).

[29] R. Lafaye, T. Plehn, M. Rauch and D. Zerwas, Eur. Phys. J. C **54**, 617 (2008).

[30] N. Arkani-Hamed, M. Porrati and L. Randall, JHEP **0108**, 017 (2001); R. Rattazzi and A. Zaffaroni, JHEP **0104**, 021 (2001); R. Contino, Y. Nomura and A. Pomarol, Nucl. Phys. B **671**, 148 (2003); K. Agashe, R. Contino and A. Pomarol, Nucl. Phys. B **719**, 165 (2005); R. Contino, L. Da Rold and A. Pomarol, Phys. Rev. D **75**, 055014 (2007).